

Function of Redox-Active Tyrosine in Photosystem II

Hiroshi Ishikita and Ernst-Walter Knapp

Institute of Chemistry and Biochemistry, Free University of Berlin, Berlin, Germany

ABSTRACT Water oxidation at photosystem II Mn-cluster is mediated by the redox-active tyrosine Y_Z . We calculated the redox potential (E_m) of Y_Z and its symmetrical counterpart Y_D , by solving the linearized Poisson-Boltzmann equation. The calculated $E_m(Y/Y^-)$ were +926 mV/+694 mV for Y_Z/Y_D with the Mn-cluster in S2 state. Together with the asymmetric position of the Mn-cluster relative to $Y_{Z/D}$, differences in H-bond network between Y_Z ($Y_Z/D1\text{-His}^{190}/D1\text{-Asn}^{298}$) and Y_D ($Y_D/D2\text{-His}^{189}/D2\text{-Arg}^{294}/CP47\text{-Glu}^{364}$) are crucial for $E_m(Y_{Z/D})$. When $D1\text{-His}^{190}$ is protonated, corresponding to a thermally activated state, the calculated $E_m(Y_Z)$ was +1216 mV, which is as high as the E_m for $P_{D1/D2}$. We observed deprotonation at $CP43\text{-Arg}^{357}$ upon S-state transition, which may suggest its involvement in the proton exit pathway. $E_m(Y_D)$ was affected by formation of P_{D2}^+ (but not P_{D1}^+) and sensitive to the protonation state of $D2\text{-Arg}^{180}$. This points to an electrostatic link between Y_D and P_{D2} .

INTRODUCTION

O_2 on earth is generated by water oxidation at the Mn-cluster of the photosynthetic protein-pigment complex, photosystem II (PSII). The photosynthetic reaction in PSII is initialized by light absorption, resulting in electronic excitation that is ultimately converted to chemical potential by a charge separation process at the P680 chlorophyll *a* (Chl*a*) of the PSII reaction center (RC). Charge separation leads to formation of an oxidized positively charged radical $P680^{++}$ while the released electron travels along the electron transfer (ET) chain. The ET chain is located in the $D1/D2$ -chain harboring a quasi-dimer Chl*a* ($P_{D1/D2}$), and pairs of accessory Chl*a* ($Chl_{D1/D2}$), of pheophytin*a* ($Pheo_{D1/D2}$) and of plastoquinone ($Q_{A/B}$). In intact PSII, $P680^{++}$ is reduced by the redox-active tyrosine $D1\text{-Tyr}^{161}$ (Y_Z), which is subsequently reduced by an electron from the Mn-cluster. An overview of the location of these cofactors in the complete PSII protein complex is shown in Fig. 1.

Sequential excitations of P680 drive the redox state of the Mn-cluster from the lowest S0 to the highest oxidized state S4. Release of O_2 as a product of water oxidation is associated with transition from S4 to S0 that completes the redox cycle. Y_Z possesses $D1\text{-His}^{190}$ while the symmetrical counterpart $D2\text{-Tyr}^{160}$ (Y_D) possesses $D2\text{-His}^{189}$ as H-bond partner (Fig. 2). The apparent proximity of Y_Z to the Mn-cluster (edge-to-edge distance between Mn-cluster and Y_Z is 5 Å (1)) and its redox-activity supports its significant role in water oxidation at the Mn-cluster. It is a matter of debate whether the role of Y_Z in water oxidation is to function as hydrogen abstractor (2) or electrostatic promoter (3). The exit pathway of protons released upon water oxidation (4) as supported by the recent crystal structure of PSII (1,5,6) is a

new aspect to be considered. The other tyrosine Y_D is 28 Å from the Mn-cluster (1) and can therefore not directly be involved in water oxidation occurring at the Mn-cluster. Nevertheless, it plays an important role in tuning the energy of the charge state of P680 and of the S-states of the Mn-cluster before ET from Y_Z to P680, as has been discussed (7–9).

There are, in principle, three possible mechanistic patterns for the involvement of tyrosine in the redox reaction between P680 and Mn-cluster. These are the following redox reactions with corresponding redox pairs (notation: YH, protonated neutral species; Y^- , deprotonated anion; YH^+ , protonated cationic radical; Y^\cdot , deprotonated neutral radical):

1. $Y^- \rightarrow Y^\cdot + e^-$ involving Y/Y^- ($E_m(Y/Y^-) = +680$ mV, measured for *N*-acetyl-L-tyrosinamide).
2. $YH \rightarrow Y^\cdot + H^+ + e^-$ involving Y/YH with $pK_{a,red}$ of 9.6 referring to YH ($E_m(Y/YH) = +970$ mV, measured for *N*-acetyl-L-tyrosinamide in aqueous solution at pH 5.0).
3. $YH \rightarrow YH^+ + e^-$ involving YH^+/YH with $pK_{a,ox}$ of -2 referring to YH^+ ($E_m(YH^+/YH) = +1380$ mV, measured for *N*-acetyl-L-tyrosinamide; reviewed in (10)).

In the following, the pK_a for tyrosine is generally used as $pK_{a,red}$, if not otherwise specified. In aqueous solution, the availability of these three possible redox reactions depends predominantly on pH. In a protein, these reactions can also be controlled by its environment as, for instance, H-bond network, presence of charged residues, and cofactors.

For efficient function of PSII, $E_m(Y_Z)$ should lie between the E_m values of P680 (+1110–1300 mV) (11,12) and water (+820 mV). Based on the equilibrium constants of the redox reactions involving Y_Z and Y_D and the pH-dependence of these redox reactions, the $E_m(Y_Z)$ and $E_m(Y_D)$ were estimated to be $\sim +970$ mV (13) and +720 to +760 mV (13,14), respectively. On the other hand, equilibrium constants measured for the redox reaction between P680 and

Submitted November 1, 2005, and accepted for publication February 2, 2006.

Address reprint requests to E. W. Knapp, Tel.: 49-30-83-85-43-87; E-mail: knapp@chemie.fu-berlin.de.

H. Ishikita's present address is Dept. of Chemistry, The Pennsylvania State University, 104 Chemistry Building, University Park, PA 16802.

© 2006 by the Biophysical Society

0006-3495/06/06/3886/11 \$2.00

doi: 10.1529/biophysj.105.076984

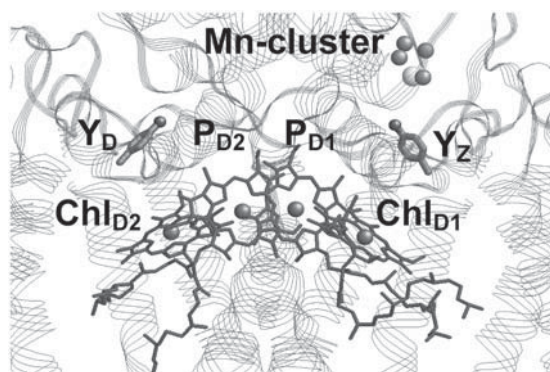


FIGURE 1 Location of the Mn-cluster (manganese, dark-shaded spheres; calcium, light-shaded sphere), Y_Z, Y_D (side chains only, light-shaded spheres for oxygen), and four Chl a P_{D1/D2} and Chl_{D1/D2} in the reaction center (dark-shaded) of PSII. Polypeptide chains are shown by ribbon bands.

Y_Z suggest that $E_m(Y_Z)$ operating in the ET process between P680 and Y_Z should be relatively high, yielding a value of +1200 mV, which is ~100 mV below $E_m(P680)$ (3,15) (reviewed in (10)). However, the mechanism of how the Y_{Z/D} environment of PSII shifts $E_m(Y_{Z/D})$ needs further investigations to be clarified (see discussion in (9)). To obtain a stable Y_Z radical, many investigations on its function were, for technical reasons, performed on Mn-depleted PSII, since under these circumstances spectroscopic signals originating from Y_{Z/D} could be detected under stationary conditions. However, it was suggested that Mn-depleted PSII samples could be subject to critical changes in conformation or H-bond network (see for instance (16,17)). Hence, an interpretation of these experiments involves uncertainties.

Recently, higher resolution crystal structures of PSII isolated from the thermophilic cyanobacterium *Thermosynechococcus elongatus* were obtained, revealing side-chain

arrangements and their interactions with redox-active cofactors (1,18). Here, we report on $E_m(Y_{Z/D})$ calculated by solving the linearized Poisson-Boltzmann (LPB) equation for the whole PSII complex based on the PSII crystal structure (1), taking into account the atomic coordinates of all amino-acid residues and bound cofactors. All computations presented here were performed under the same conditions and parameterization as in previous computations on PSII (for instance, (19,20)).

METHODS

Coordinates

In our computations, all atomic coordinates were taken from the crystal structure of PSII from thermophilic cyanobacterium *T. elongatus* at a 3.5 Å resolution (PDB: 1S5L) (1). Hydrogen atom positions were energetically optimized with CHARMM (21), while positions of all nonhydrogen atoms were fixed and all titratable groups were kept in their standard protonation states, i.e., acidic groups ionized and basic groups (including titratable histidines) protonated. Simultaneously, Chl a, Pheo a, and Q_{A/B} were kept in the neutral charge redox states. Histidines that are ligands of Chl a were treated as nontitratable with neutral total charge.

Atomic partial charges

Atomic partial charges of amino acids were adopted from the all-atom CHARMM22 (22) parameter set. To account implicitly for the presence of a proton, the charges of acidic oxygens were both increased symmetrically by +0.5 unit charges. Similarly, instead of removing a proton in the deprotonated state, all hydrogen charges of the basic groups of arginine and lysine were diminished symmetrically by a unit charge in total. The atomic charges for the redox-active tyrosine were adopted from Popovic et al. (23); deprotonated with negative charge (Y⁻); deprotonated radical with neutral charge (Y[•]) in the redox pair Y[•]/Y⁻; protonated with neutral charge (YH); and protonated radical with positive charge (YH^{•+}) in the redox pair YH^{•+}/YH.

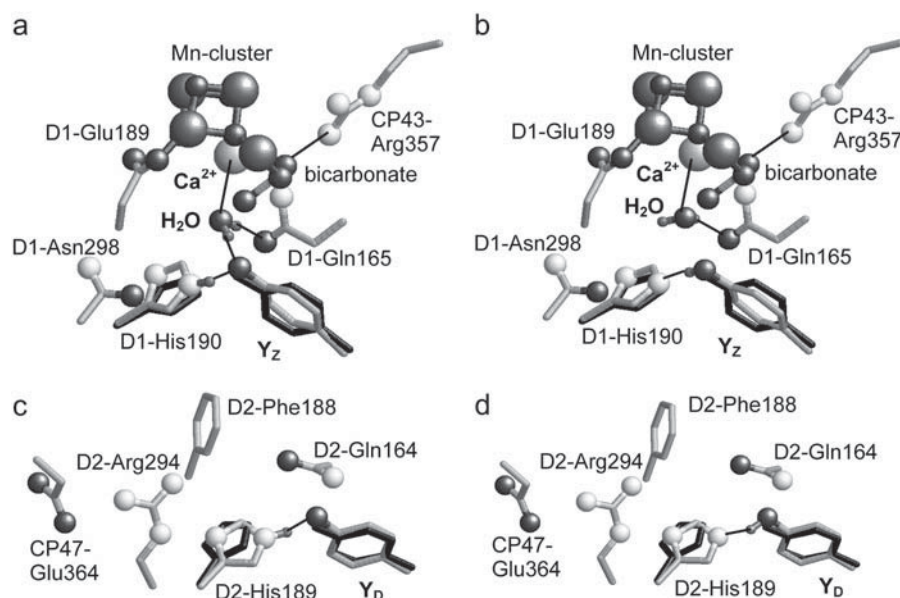


FIGURE 2 H-bond network around Y_{Z/D}. Energetically optimized atomic coordinates for (a) deprotonated Y_Z, (b) protonated Y_Z, (c) deprotonated Y_D, and (d) protonated Y_D. Only for D1-His¹⁹⁰/D2His¹⁸⁹ and H₂O, polar hydrogen atoms involved in H-bonds are displayed explicitly by small-sized dark-shaded spheres. Nitrogen atoms are displayed by medium-sized light-shaded spheres, oxygen atoms by medium-sized dark-shaded spheres, and Mn and Ca ions are shown by large spheres (manganese, dark-shaded; calcium, light-shaded). Original positions of Y_{Z/D} and D1-His¹⁹⁰/D2-His¹⁸⁹ from the PSII crystal structure are shown by dark-shaded sticks; energetically optimized positions are shown in light shading. Orientations of H-atoms and some H-bonds are indicated by thin lines.

Molecular systems and dielectric media

Although a formidable and still unsolvable task, a complete description of a molecular system (as for instance, a protein immersed in solvent) can in principle be achieved by solving the Schrödinger equation for all atoms comprising electrons and nuclei for a statistical average of conformations. In such a complete description there is no space to introduce a continuum dielectric medium. The other extreme is to ignore the atomic structure and conformations of the molecular system completely. In this case the dielectric medium is necessary to describe polarization effects emerging from of the dipoles in the molecular system, which create a reaction field in response to explicit charges or dipoles. Polarization effects have contributions not only from distortions of electronic wave functions (electron polarization) and conformational changes of the nuclei (nuclear polarization), but also from nonhomogeneous distributions of charged groups and their variations (for instance, titratable groups in a protein).

In theoretical computations, often mixed models are used where part of the molecular structure is treated explicitly, while the nonexplicit parts are considered by an effective dielectric medium. Here as in a number of preceding studies (19,20,24–26), we consider the atomic partial charges and variations of charge pattern due to titratable groups explicitly, while we ignore electronic polarization and nuclear polarization. The latter is true, since we consider only a single conformation, which is directly related to the atomic coordinates of the protein crystal structure. Based on a number of studies (19,20,24–26) we obtained best results for redox-active and titratable groups with a dielectric constant of $\epsilon_p = 4$ inside the protein and $\epsilon_w = 80$ outside to model the polarization of bulk water. The same values were used in computational studies of other groups (27,28). If we ignore the influence of charged groups and their variations in a protein, the value of the dielectric constant would vary depending on the molecular system considered and exhibit spatial dependencies related to the distribution of titratable residues. It should be noted here that a dielectric constant used for such mixed models is a model parameter like atomic partial charges but not a quantity directly amenable to experimental measurement.

In other computational work, also larger values than $\epsilon_p = 4$ were used for the protein dielectric constant, for instance $\epsilon_p = 20$ (29). Since the dielectric constant accounts for the molecular components that are not explicitly modeled, a description with lower dielectric constant is superior as long as the agreement with experimental data is of the same level. In this respect it is interesting to note that considering conformational flexibility (i.e., including nuclear polarization) by energy minimization yields best results by lowering the dielectric constant from 4 to 2 to account for only electron polarization (30).

Experimental determinations of the static dielectric constant in a molecular system are generally based on the assumption to describe polarization effects solely by a dielectric continuum. In bacterial RC the dielectric constant was determined by measuring the Stark effect (31). In these measurements the influence of electrostatic interactions of a chromophore with the protein environment is probed in terms of a double difference in energies, namely ground and electronic excited state energies in presence and absence of a strong external electrostatic field. For such double differences the direct influence of charged groups cancels, if they do not change their charge state with the external electrostatic field. However, such changes are likely to occur for titratable residues. Interpreting such contributions in terms of an inhomogeneous dielectric medium would result in a spatially varying dielectric constant. The measured values of ϵ_p in the bacterial RC vary between 2.1 and 9.5 (31), presumably due to variations in the protonation pattern of titratable residues. However, the average of the measured dielectric constants is close to the value used in our electrostatic energy computations.

Protonation pattern and redox potential

Our computation is based on the electrostatic continuum model treated by solving the LPB equation with the program MEAD (32). To facilitate a

direct comparison with previous computational results, we used uniformly the same computational conditions and parameters such as atomic partial charges and dielectric constants (for instance, (19,20)). To obtain absolute values of the $E_m(Y)$ in the protein, we calculated the electrostatic energy difference between the two redox states of tyrosine in a reference model system with known experimental E_m . The shift of E_m in the protein relative to the reference system was added to the known E_m . As reference model system, the following solution E_m s versus normal hydrogen electrode were used: $E_m(Y/Y^-) = +680$ mV for one-electron reduction; and $E_m(YH^+/YH) = +1380$ mV for one-electron oxidation in aqueous solution (10). Although the radical pair of YH^+/YH could be also relevant for the radical state of $Y_{Z/D}$ in PSII, in this study we did not focus on this radical pair (see Discussion). The redox states of all other cofactors (i.e., Car, Chl_a, Pheo_a, quinone) were kept in their neutral charge state. Cytochrome b559 and cytochrome c550 were kept in the reduced state. Specifically, unless titrated, Y_Z and Y_D were kept in the neutral charge state. The ensemble of protonation patterns was sampled by a Monte Carlo method with our own program Karlsberg (B. Rabenstein, Karlsberg Online Manual, [http://agnapp.chemie.fu-berlin.de/karlsberg/\(1999\)](http://agnapp.chemie.fu-berlin.de/karlsberg/(1999))). All computations were performed at 300 K with pH 7.0 and an ionic strength of 100 mM. The LPB equation was solved using a three-step grid-focusing procedure with 2.5 Å, 1.0 Å, and 0.3 Å resolution. The Monte Carlo sampling yielded the probabilities $[A_{ox}]$ and $[A_{red}]$ of the two redox states of molecule A. The E_m was evaluated from the Nernst equation. A bias potential was applied to obtain an equal amount of both redox states ($[A_{ox}] = [A_{red}]$), yielding the redox midpoint potential E_m as the resulting bias potential. For convenience, the computed E_m was given with mV accuracy, without implying that the last digit is significant. In general, a few 10 mV in E_m is in a sufficiently reproducible range of our computational method (see, for instance, (33)). With the Henderson-Hasselbalch equation, the pKa can be calculated as the pH where the concentration of $[A_{deprotonated}]$ and $[A_{protonated}]$ are equal. For further information about computational procedure and error estimate, see our previous work for E_m (for instance, (19,20)) and pKa (for instance, (34,35)).

Modeling water between the Mn-cluster Ca^{2+} and Y_Z

The existence of a water molecule located in H-bond distance to Y_Z and D1-His¹⁹⁰ has been proposed to play a significant role in the redox reaction of Y_Z for years. Although crystal structures of PSII could not reveal water molecules due to their limited resolutions, the crystal structure of PSII (1,6) indicates a possible water binding site X21 at Ca^{2+} of the Mn-cluster and Y_Z , which is in agreement with ¹⁸O isotope exchange measurements that pointed to a Ca-bound water (36). The exact mechanism of PSII water oxidation as mediated by Y_Z and the Mn-cluster remains a matter of debate, but the majority of the proposed mechanisms seem to place at least one water molecule in the neighborhood of Y_Z and the Mn-cluster (37,38).

We modeled this water molecule in the vicinity of Y_Z and optimized its geometry energetically with CHARMM (21) while all other atomic coordinates except $Y_{Z/D}$ and D1-His¹⁹⁰/D2-His¹⁸⁹ were fixed. Both $Y_{Z/D}$ were treated as 1), negatively charged deprotonated tyrosine (Y^- model, Fig. 2, *a* and *c*) (17,39,40); or 2), neutral protonated tyrosine (YH model, Fig. 2, *b* and *d*) (10,41,42). Alternatively, in a geometry optimization with positively charged tyrosine YH^+ , the side chains of Y_Z and D1-His¹⁹⁰ moved apart, disrupting the common H-bond (data not shown), rendering this H-bond unstable. Hence YH^+ might be relevant only as a transient state.

The exact PSII conformations for $Y_{Z/D}$ radical states are so far unknown. One of the most relevant studies to refer to this issue is a structural refinement of Högbom et al. (43) for a tyrosine radical position in a single crystal of ribonucleotide reductase R2 protein by combined x-ray and high-field EPR crystallography (43). Although the protein environment of the tyrosine radical in the two proteins are different, in the R2 protein a displacement of the side chain was observed predominantly at this tyrosine upon generation of its radical state. Therefore, in our study we released the

atomic coordinates only for the minimum set of relevant residues, i.e., Y_Z/D1-His¹⁹⁰ (Y_D/D2-His¹⁸⁹) pair. As a consequence of the geometry optimization, atom pair distances of tyrosines and histidines were changed by 0.1–0.8 Å with an RMS deviation of 0.63 Å for the Y[−] model and 0.51 Å for the YH model with respect to the side-chain atoms (excluding hydrogen and backbone atoms; see Table 1). These displacements of side chains are in the same range as those observed in the generation of tyrosine radicals in the R2 protein (PDB 1MXR; see also Fig. 5 in (43)). The energy-optimization procedure did not alter the O_Y–N_{His} distance for Y_Z/D1-His¹⁹⁰. In contrast, the corresponding Y_D–His¹⁸⁹ atom pair distance decreased by 0.4 Å to 2.6 Å, which is nearly identical to the distance of 2.7 Å for the Y_Z/D1-His¹⁹⁰ pair. In the geometry-optimized PSII structure, the water molecule is 3.0 Å from the Ca²⁺ ion at the Mn-cluster, 2.6 Å from the hydroxyl oxygen atom of Y_Z, and 3.0 Å from the side-chain oxygen atom of D1-Gln¹⁶⁵ (Fig. 2). This completely agrees with the suggestion of a Ca-bound water that is H-bonded to Y_Z (5,37,38). We obtained the H-bond formation between the modeled water and D1-Gln¹⁶⁵, which agrees with a suggestion in McEvoy and Brudvig (37). The optimized atomic coordinates of Y_Z, D1-His¹⁹⁰, and the X21 water as well as Y_D and D2-His¹⁸⁹ used in this study are available online as Supplementary Material (files YZ_deprot.pdb and YD_deprot.pdb for Y[−] model, and YZ_prot.pdb and YD_prot.pdb for YH model, respectively).

The dielectric constant for the explicit modeled water X21 was set to $\epsilon_p = 4$, i.e., to the same value as in the protein volume, in contrast to $\epsilon_w = 80$ used for bulk water. With higher dielectric constant, electrostatic interactions are shielded more efficiently, as it is for instance the case in bulk water. The screening ability of electrostatic interactions caused by a single, explicitly modeled water molecule buried in the protein can be understood by reorientation of its dipole to stabilize atomic charges in the protein. One focus in this study is to investigate explicit H-bond pattern of water X21 to protein cofactors. Atomic coordinates of this modeled water near Y_{ZD} were energetically optimized to form explicit H-bonds with the protein environment, which can establish sufficient electrostatic screening of protein charges in the neighborhood. However, the electrostatic screening is effective only if the water volume possesses a low dielectric constant as, for instance, $\epsilon = 4$.

TABLE 1 Geometry of the H-bond network at Y_{ZD} after energy optimization of Y_{ZD} and D1-His¹⁹⁰/D2-His¹⁸⁹ side chains in the presence of negatively charged tyrosine

Atom pair	Distance [Å]	
	Original*	Optimized†
Y _Z		
N _{His} [‡] –O _{ηYZ} [§]	2.7	2.7
N _{His} [‡] –O _{δAsn} [¶]	3.3	4.1
O _{bicarbonate} –O _{ηYZ} [§]	3.4	2.9
O _{H2O} –O _{ηYZ} [§]	(2.7)	(2.6)
O _{H2O} –N _{His} [‡]	(3.4)	(3.0)
Y _D		
N _{His} [‡] –O _{ηYD} [§]	3.0	2.6
N _{His} [‡] –N _{Arg} ^{**}	2.4	3.2
N _{His} [‡] –N _{Arg} ^{**}	3.2	3.5

*Based on the atomic coordinates of the PSII crystal structure (1).

†Based on energy optimized atomic coordinates of PSII with CHARMM (see text).

‡D1-His¹⁹⁰ for Y_Z and D2-His¹⁸⁹ for Y_D.

§Hydroxyl oxygen atom of Y_{ZD}.

¶Side-chain oxygen atom of D1-Asn²⁹⁸.

||The H₂O molecule was placed in the PSII crystal structure between the Mn-cluster Ca²⁺ and Y_Z. It was first energetically optimized alone and subsequently together with Y_Z and the D1-His¹⁹⁰ side chains.

**Side-chain nitrogen atom of D2-Arg²⁹⁴.

Evaluation of $E_m(Y_{ZD})$ with/without energy minimization

When we used the original atomic coordinates from the crystal structure, we calculated $E_m(Y_Z/Y_Z^-)$ and $E_m(Y_D/Y_D^-)$ to be +944 mV and +586 mV at pH 6 for the S₂ state, respectively. After energy minimization of the side chains of Y_{ZD} and D1-His¹⁹⁰/D2-His¹⁸⁹, we obtained at pH 6 for the S₂ state $E_m(Y_Z/Y_Z^-) = +985$ mV and $E_m(Y_D/Y_D^-) = +742$ mV (see main text). The E_m difference between Y_Z and Y_D was formerly estimated to be +240 meV from the equilibrium constant for Y_Z/Y_D (14) or +210 meV from the equilibrium constants for Y_Z/S_{2/I} and Y_D/S_{2/I} (13). From this E_m difference, Vass and Styring (13) estimated $E_m(Y_Z/Y_Z^-)$ and $E_m(Y_D/Y_D^-)$ to be ~+970 mV and +760 mV, respectively (13). The E_m difference $E_m(Y_Z) - E_m(Y_D)$ of +243 mV as well as the absolute values of $E_m(Y_{ZD})$ obtained in our computations using the energy-minimized coordinates are in good agreement with the estimated values of Vass and Styring (13). On the other hand, using the original atomic coordinates from the PSII crystal structure, the calculated $E_m(Y_D/Y_D^-)$ is lower by ~150 mV than by using the energy-minimized coordinates. In contrast, the calculated $E_m(Y_Z/Y_Z^-)$ is nearly the same in the two atomic coordinate sets. The resulting E_m difference of +358 mV between Y_Z and Y_D in the original atomic coordinates is by ~100 mV larger than the corresponding values from the estimate of Vass and Styring (13) and our computations using the atomic coordinates from the energy-minimized model. Analyzing the two structures in atomic detail, it becomes evident that the low value of $E_m(Y_D/Y_D^-)$ in the original PSII structure originates mainly from the relatively large N_{His}–O_{ηYD} distance of 3.0 Å in the PSII crystal relative to the smaller distance of 2.6 Å in the geometry-optimized PSII structure (Table 1). The same distance of 2.6 Å was also obtained by DFT computations of Faller et al. (44) considering the same H-bond pattern between Y_D and D2-His¹⁸⁹. Indeed, the distance of 2.6 Å is nearly identical to the corresponding distance of 2.7 Å in the Y_Z side of the PSII crystal structure (Table 1). Although the N_{His}–O_{ηTYR} in the Y_D side was thus affected, it is quite remarkable that the same energy-minimization process did not alter the corresponding distance in the Y_Z side. Despite the alteration in $E_m(Y_D)$ by the energy minimization, the other features (e.g., protonation pattern in PSII) remained unchanged in our computation. Therefore, in the following part, we focused on the computation based on the atomic coordinates with these side chains being energetically optimized.

RESULTS AND DISCUSSION

$E_m(Y_Z/Y_Z^-)$

At pH 6 in the S₂ state, the calculated $E_m(Y_Z/Y_Z^-)$ is +985 mV, which agrees with the measured $E_m(Y_Z)$ of ~+970 mV, as reported by Vass and Styring (13). This value is also close to $E_m(Y/Y) = +970$ mV measured for the neutral tyrosine radical in aqueous solution at pH 5.0 (10,45). At pH 7, the calculated $E_m(Y_Z/Y_Z^-)$ are +926 mV (+959 mV) in the S₂ (S₃) state (Table 2). EPR signals from a tyrosine radical in PSII were assigned to Y_Z interacting with the Mn-cluster in the S₂ state and its pH-dependence observed in these experiments was attributed to a pH-dependent $E_m(Y_Z)$ (46). In our computations, we observed pH-dependence of $E_m(Y/Y^-)$ for Y_Z and Y_D with a slope of ~−60 mV/pH in the S₂ state.

When we calculated $E_m(Y_Z/Y_Z^-)$ in the S₂ state at pH 7.0 (i.e., at [Y] = [Y[−]] = 0.5), D1-His¹⁹⁰ was to 50% protonated, implying a neutral charge state of the residue pair Y_Z/D1-His¹⁹⁰. On the other hand, a number of experimental studies proposed that D1-His¹⁹⁰ is protonated (i.e., positively charged) before relaxing to the S₂ state (reviewed in (47)).

TABLE 2 Computed $E_m(Y_{Z/D})$ in [mV] at pH 7.0

Redox couple	Mn-cluster S-state	$E_m(Y_Z)$	$E_m(Y_D)$
Y^+/Y^{*-}	S0	+932	+686
	S1	+931	+689
	S2	+926	+694
	S3	+959	+702
	Mn-depleted [†]	+780	+685
Y^+/Y^*	S2	+1669	+1907

*For the E_m values used as reference model system, see Tommos and Babcock (10).

[†]All the titratable groups in PSII were titrated, as was done in computations with intact Mn-cluster.

In our computation, at pH 7 D1-His¹⁹⁰ was fully protonated if Y_Z was fully reduced as tyrosinate (Y_Z^-) for all S-states investigated.

Considering protonated D1-His¹⁹⁰, which presumably prevails in a thermally activated state of PSII, we obtained $E_m(Y_Z/Y_Z^-) = +1216$ mV. Quite interestingly, the $E_m(Y_Z)$ value obtained in presence of a fully protonated D1-His¹⁹⁰ is nearly as high as $E_m(P680)$ of $\sim +1200$ to $+1300$ mV (11,12). The proximity between $E_m(Y_Z)$ and $E_m(P_{D1/D2})$ is consistent with a small E_m difference between P680 and Y_Z , governing the ET between these cofactors in the nanosecond time domain before possible structural relaxation (3,15). This E_m difference is time-dependent and increases in the microsecond time regime, yielding finally under equilibrium conditions in the S2 state $E_m(Y_Z) = +970$ mV (13) ($E_m(Y_Z) = +985$ mV computed in this study). Thus, in our computational model, a change in protonation at D1-His¹⁹⁰ (using the same atomic coordinates from the PSII crystal structure (1)) has a predominant impact on $E_m(Y_Z)$, yielding an upshift of 260–290 mV. This mechanism may be necessary to reduce P680⁺ by Y_Z quickly in the nanosecond time regime (48).

$E_m(Y_D/Y_D^-)$

At pH 6 in the S2 state, the calculated $E_m(Y_D/Y_D^-)$ is +742 mV. At pH 7 we calculated $E_m(Y_D/Y_D^-)$ to be +694 mV in the S2 state and +702 mV in the S3 state (Table 2). The experimentally estimated $E_m(Y_D/Y_D^-)$ lies between +720 and +760 mV according to redox titration with strong oxidants (14) or from determination of the E_m difference, $E_m(Y_Z) - E_m(Y_D)$ (13). Interestingly, these estimated $E_m(Y_D/Y_D^-)$ in PSII (13,14) are very similar to the $E_m(Y^+/Y^-)$ value in aqueous solution where it was measured to be +680 mV for pH >9.9 independent of pH (10) although the very polar solvent environment differs considerably from the PSII environment. The different redox behavior of the two symmetry-equivalent tyrosines seems to be mainly due to the asymmetric location of the Mn-cluster being close to Y_Z and distant to Y_D with edge-to-edge distances of 5 Å and 28 Å, respectively. As observed in $E_m(Y_Z/Y_Z^-)$, we found also $E_m(Y_D/Y_D^-)$ to be pH-dependent with ~ -60 mV/pH in our electrostatic energy computations.

Model of ET from Y_Z to P680⁺ in intact PSII

The calculated $E_m(YH^+/YH)$ were +1576 mV for Y_Z and +1804 mV for Y_D at pH 7 in the S2 state, which indicates less stability of YH^+/YH relative to the deprotonated redox pair Y^+/Y^- . In agreement with our computed results on $E_m(YH^+/YH)$, Tommos and Babcock (10) also estimated $E_m(YH^+/YH)$ for the PSII protein environment to be +1680 mV to +1830 mV (10). These large values for $Y_{Z/D}$ are not only far from +970 mV (+985 mV) obtained by Vass and Styring (13) (computed in this study for $E_m(Y_Z/Y_Z^-)$), but also far from $E_m(Y_Z/Y_Z^-) = +1216$ mV, computed for protonated D1-His¹⁹⁰.

Although we obtained for $E_m(Y_Z)$ values as low as +985 and +1216 mV only by considering the redox pair Y_Z/Y_Z^- , it does not exclude the possibility that Y_Z is protonated (Y_ZH) before its radical reaction, as found in Fourier-transform infrared (FTIR) studies (41,42). Hence, our computations suggest that Y_Z^- relative to Y_Z is energetically more stabilized than YH^+ relative to Y_ZH , such that the redox pair Y_Z/Y_Z^- is likely more relevant than Y_ZH^+/Y_ZH .

Tommos and Babcock (10) argued that Y_Z/Y_Z^- is not the functional redox pair in PSII unless positive charges near Y_Z lower the pKa of Y_ZH to values <5, concluding that Y_Z/Y_Z^- is unlikely to be the relevant redox pair (10). However, we remark that not only positive charges but also appropriate H-bonds with the titratable redox-active Y_Z are able to lower the pKa and stabilize its anionic form. A number of studies suggest that, in the Y_Z side, a Ca-bound water exists (1,6, 37,38). Indeed, the fixation of a water at the Ca²⁺ of the Mn-cluster results in a strong H-bond between this water and the hydroxyl oxygen of Y_Z (Fig. 2 a and Table 3). Due to the H-bond with this Ca-bound water, we obtained a pKa of 7.4 for Y_ZH (Fig. 3, panels 1 and 4), which is relatively low with respect to the pKa of 9.6 for tyrosine in aqueous solution. However, this pKa value for Y_Z is in agreement with the pKa values of 7.0–8.3 derived by Ahlbrinck et al. (3) and Diner et al. (40) from the ET rate involving Y_Z and P680⁺. A further support for this pKa is the FTIR result of Berthomieu et al. (42), which observed the disappearance of a band at 1238–1255 cm⁻¹ with an apparent pKa of ~ 8 –9, corresponding to a $\delta(\text{COH})$ tyrosine-bending mode (cited as personal communication in (49)). When Y_Z is equilibrated in the Y_ZH/Y_Z^- states then we calculated pKa of D1-His¹⁹⁰ to be 6.6 (Fig. 3, panel 1). Hence, the Ca-bound water plays a role in stabilizing transient Y_Z states such as $Y_Z^{\delta-}$ (where Y_Z

TABLE 3 Influence of P_{D1}P_{D2} and D2-Arg¹⁸⁰ charge states on $E_m(Y_{Z/D})$ at pH 7.0 in the S2 state

Charge state	$E_m(Y_Z)$ [mV]	$E_m(Y_D)$ [mV]
P _{D1} ⁰ P _{D2} ⁰	+926	+694
P _{D1} ⁺ P _{D2} ⁰	+918	+732
P _{D1} ⁰ P _{D2} ⁺	+924	+802
P _{D1} ⁰ P _{D2} ⁰ with D2-Arg ¹⁸⁰ deprot.	+926	+564

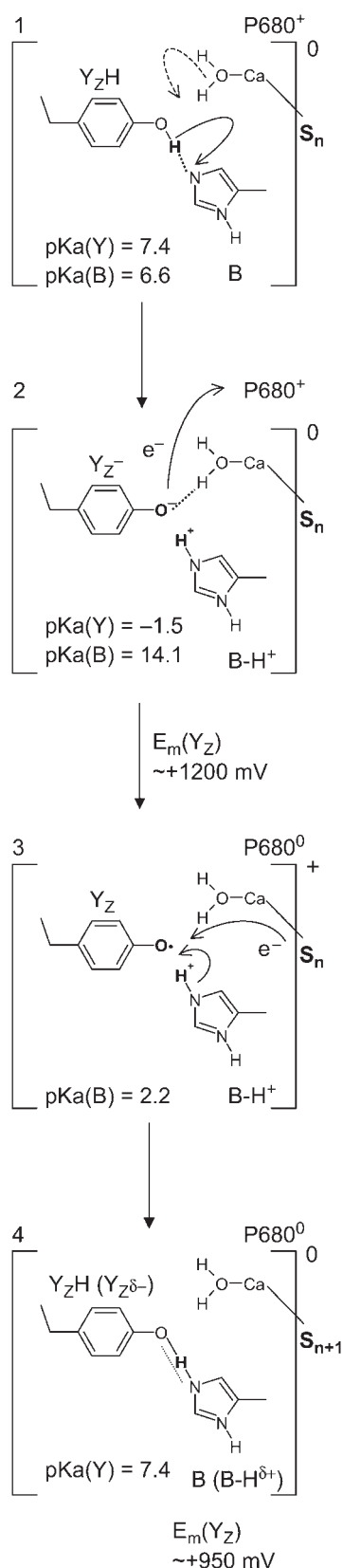


FIGURE 3 Scheme for ET from Y_Z to P680. Y and B stand for Y_Z and D1-His¹⁹⁰, respectively, and the calculated pK_a values of Y and B for these residues at each step are listed in the scheme.

and D1-His¹⁹⁰ share a proton, thus being in the neutral charge state) or Y_Z⁻, which otherwise would be very unstable.

We interpreted our results for Y_Z/Y_Z⁻ by the following redox reaction scheme of Y_{Z/D} visualized in Fig. 3:

1. In the initial state, Y_ZH dissociates the phenolic proton (Fig. 3, panel 1).
2. The presence of the Ca-bound water stabilizes the Y_Z⁻ state transiently with fully protonated D1-His¹⁹⁰ (BH⁺) ($E_m(Y_Z) = +1216 \text{ mV}$) (Fig. 3, panel 2). This step is particularly unstable and should therefore exist only transiently, since according to our calculated pK_a Y_Z and B are an extremely strong acid and base, respectively. Since in the initial state proton release of Y_ZH, producing Y_Z⁻ (Fig. 3, panel 2), is immediately quenched by an oxidation process where Y_Z⁻ decays to the neutral radical state Y_Z, the intermediate reaction state Y_Z⁻ displayed in Fig. 3, panel 2, is often not considered explicitly. Thus, the resulting net redox reaction of these two steps involves Y_Z/Y_ZH (Fig. 3, panels 1–3).
3. For the neutral radical state Y_Z, the pK_a of B is 2.2, still considerably low (Fig. 3, panel 3). As a consequence, the protonated BH⁺ becomes unstable, donating its proton to the neutral radical Y_Z. In this proton transfer step, the residue pair Y_Z and B remains positively charged.
4. This energetically unfavorable charge state relaxes by charge compensation receiving an electron from the Mn-cluster, which in turn changes from state S_n to S_n+1 (Fig. 3, panel 4).

It is a matter of debate whether the H-bond between the Ca-bound water and Y_Z remains unchanged even in this state (Fig. 3, panel 4), but if it does, then it leads to a protonated Y_Z and a deprotonated B, which are H-bonded [B...HY_Z] or alternatively to a partially polarized (but also uncharged) species [B-H^{δ+}...Y_Z^{δ-}] where the proton is delocalized in the H-bond, yielding $E_m(Y_Z) = +926$ for the S2 state (+959 mV for the S3 state) (Fig. 3, panel 4). Hereby, our computations yielded a partially protonated Y_Z (~0.7 H⁺), which as a consequence carries a fractional negative charge. This fractional negative charge is practically completely neutralized by a complementary fractional protonation of D1-His¹⁹⁰ (~0.3 H⁺). This polarized H-bond resembles the tyrosinate intermediate model (17,39,40). Hence, in FTIR measurements the predominantly protonated Y_Z species may still be detected as protonated Y_ZH (41,42).

$E_m(Y_ZH^+/Y_ZH)$ in the Mn-depleted PSII model

Although it has been suggested that Mn-depleted PSII may possess considerably different H-bond pattern around Y_Z compared to those in intact PSII (16,17), we tentatively modeled an Mn-depleted PSII by simply removing the Mn-cluster, the attached bicarbonate, Ca²⁺, and water, without considering any conformational change of the protein environment nearby. To distinguish this model from the

actual Mn-depleted PSII in vitro, we denote this model as Mn-depleted PSII model. This model possesses different H-bond pattern from those in intact PSII mainly due to the removal of the Ca-bound water, which was H-bonded to the Y_Z hydroxyl oxygen ($O_{H_2O}-O_{Tyr}$ distance of 2.6 Å) in the intact PSII. In contrast to the enormously high potential of +1576 mV for $E_m(Y_ZH^+/Y_ZH)$ in intact PSII, the Y_ZH^+/Y_ZH calculated in the Mn-depleted PSII model was lower, yielding +1264 mV. This value is also lower than +1380 mV for YH^+/YH measured in the aqueous solution (10), indicating that YH^+ is dramatically stabilized in the Mn-depleted PSII model with respect to intact PSII or aqueous solution. Furthermore, the calculated $E_m(Y_ZH^+/Y_ZH) = +1264$ mV in the Mn-depleted PSII model is approximately as high as $E_m(P680)$ of $\sim +1200$ to $+1300$ mV (11,12), implying that Y_ZH^+/Y_ZH may serve as functional electron donor to $P680^+$ in the Mn-depleted PSII. The lack of electron donor for Y_Z (i.e., the Mn-cluster) in the Mn-depleted PSII might energetically, thus, be able to accumulate Y_ZH^+ . Indeed, an interpretation that Y_ZH^+ may be the functional species in PSII was made based on EPR spectroscopy on Mn-depleted PSII (50,51). To investigate the stability of Y_ZH^+ , we calculated the $pK_{a_{ox}}$ for Y_ZH^+ . Indeed, in the Mn-depleted PSII model the calculated $pK_{a_{ox}}$ was 0.0, being increased by two units from the aqueous solution value of -2.0 . Nevertheless, this value is still too low to maintain a stable Y_ZH^+ in the Mn-depleted PSII under physiological conditions, implying that this species is likely to occur only transiently also in the Mn-depleted PSII model. An alternative interpretation for these EPR signals would be that another titratable residue, whose position is ~ 5 Å from Y_Z , is responsible for the positively charged intermediate (50). According to this interpretation of EPR studies, the involvement of this unidentified residue occurs specifically after the S2 state (50). Since the distance estimate of 5 Å is ambiguous, the involved titratable residue may be different from D1-His¹⁹⁰, as discussed in the next section. In the following, we will focus our discussion on the redox couple Y/Y^- for $Y_{Z/D}$ in intact PSII. Accordingly, the notation $E_m(Y_{Z/D})$ refers to “ $E_m(Y/Y^-)$ for $Y_{Z/D}$ ” unless otherwise stated.

Influence of CP43-Arg³⁵⁷ on $E_m(Y_Z/Y_Z^-)$

Surprisingly, our computations yielded very similar values for $E_m(Y_Z/Y_Z^-)$ in the S0 state (+932 mV) and the S2 state (+926 mV), while for the S3 state we calculated $E_m(Y_Z/Y_Z^-) = 959$ mV, which is ~ 30 mV higher than for the S2 state (Table 2). In general, the presence of two additional positive unit charges in the S2 state of the Mn-cluster relative to the S0 state should upshift $E_m(Y_Z/Y_Z^-)$ considerably. Considering the calculated difference of 30 mV for $E_m(Y_Z/Y_Z^-)$ between the S2 and S3 states, we estimate $E_m(Y_Z/Y_Z^-)$ to be as low as +860 mV in S0 state but the actual calculated $E_m(Y_Z/Y_Z^-)$ for the S0 state is

+932 mV. The apparent insensitivity of $E_m(Y_Z/Y_Z^-)$ to changes of Mn-cluster charges is due to charge compensation by a protonation change of titratable residues nearby. In this connection, we found that CP43-Arg³⁵⁷ deprotonates as the S-state shifts from S0 to S2. This residue was observed to be fully protonated in the S0 state, partially deprotonated in the S1 state, and fully deprotonated in the S2 state. Indeed, when we forced CP43-Arg³⁵⁷ to be fully deprotonated also in the S0 state, the calculated $E_m(Y_Z/Y_Z^-)$ decreased by 108 mV to +824 mV. Similarly, when we forced CP43-Arg³⁵⁷ to be fully protonated in the S2 state, the calculated $E_m(Y_Z/Y_Z^-)$ increased by 63 mV to +989 mV in the S2 state. Thus, mainly CP43-Arg³⁵⁷ is responsible for the S-state independence of $E_m(Y_Z/Y_Z^-)$ observed in our computations. Hence, the variable protonation of CP47-Arg³⁵⁷ seems to function as buffer for $E_m(Y_Z/Y_Z^-)$ during S0–S2 state transitions.

CP43-Arg³⁵⁷ is at an edge-to-edge distance of 4 Å from the Mn-cluster, close to one of the three possible substrate water binding sites, X22, which differs from the suggested Ca-bound water X21 proximal to Y_Z (1,5,6). In this location, an intermediate oxygen product before O=O bond formation of the final product O_2 might be stabilized by H-bonds with CP43-Arg³⁵⁷ as proposed in Ferreira et al. (1). These suggestions are in line with the mutation study from CP43-Arg³⁵⁷ to Ser that resulted in severely inhibited O_2 -evolution (52). Based on these arguments, McEvoy and Brudvig (37) suggested that CP43-Arg³⁵⁷ is protonated in the S-states below S2 and becomes deprotonated in the higher oxidized S-states due to its proximity to the positively charged Mn-cluster (37). This is in perfect agreement with our results on CP43-Arg³⁵⁷ protonation. Thus, as they suggested, CP43-Arg³⁵⁷ may play a central role in organizing the S-state-dependent flow of protons from the Mn-cluster, which may transfer protons to D1-Asp⁶¹ belonging to the proton exit pathway (37). Instead of the proton pathway consisting mainly in Y_Z and D1-His¹⁹⁰ as proposed by Hoganson and Babcock (2), an alternative pathway not directly via Y_Z and D1-His¹⁹⁰ was proposed by Haumann and Junge (4). The deprotonation of CP43-Arg³⁵⁷ observed here favors these alternative proton exit pathways.

Factors determining the E_m difference between Y_Z and Y_D

The E_m difference, $E_m(Y_Z) - E_m(Y_D)$, was estimated to be +240 meV from the equilibrium constant for Y_Z/Y_D (14) or +210 meV from the equilibrium constants for $Y_Z/S_{2/1}$ and $Y_D/S_{2/1}$ (13). The $E_m(Y_Z) - E_m(Y_D)$ of +232 meV in the S2 state (+257 meV in the S3 state) obtained in our computations are in good agreement with these experimental estimates. The main factors contributing to the difference between $E_m(Y_Z)$ and $E_m(Y_D)$ are differences in 1), the distance between the Mn-cluster and $Y_{Z/D}$; and 2), the H-bond pattern involving the histidines D1-His¹⁹⁰ and D2-His¹⁸⁹, respectively (see Fig. 4).

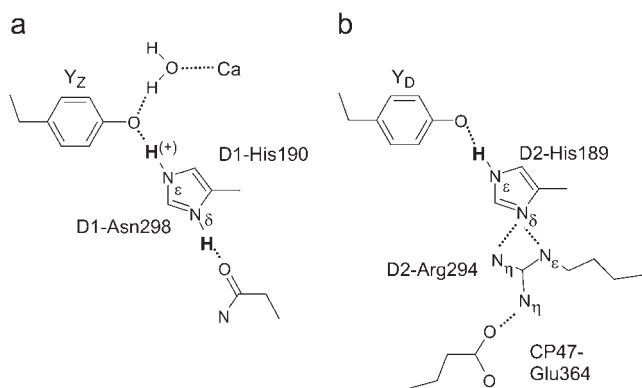


FIGURE 4 H-bond network around (a) Y_Z and (b) Y_D. Only residue side chains are shown. Dotted lines indicate H-bonds or salt-bridges. Only protons belonging to Y_{Z/D} are shown in the figure. H⁽⁺⁾ denotes the proton whose presence depends on the redox state of Y_Z.

According to the PSII crystal structure (1) the edge-to-edge distances of the Mn-cluster to Y_Z and to Y_D are 5 Å and 28 Å, respectively, which is quite different. The removal of the Mn-cluster from PSII *in vitro* could result in drastic changes of protein environment, especially around Y_Z (16,17). However, solely for the purpose of distinguishing the direct influence of Mn-cluster on $E_m(Y_{Z/D})$ from other influences, we performed electrostatic energy computations in the absence of the Mn-cluster (removing also Ca²⁺ and bicarbonate) without considering any conformational change of the remaining protein. To elucidate the actual electrostatic influence in the computation, this treatment is more appropriate. Hereby, $E_m(Y_Z)$ was downshifted by 150 mV, relative to the S2 state, to be now +780 mV (Table 2). The corresponding decrease in $E_m(Y_D)$ was only 10 mV due to the much larger distance between the Mn-cluster and Y_D. Thus, the main contribution to the E_m difference is due to the asymmetric location of the Mn-cluster relative to the D1/D2 proteins. But, there still remains an E_m difference of ~100 mV between Y_Z and Y_D.

For the computation of $E_m(Y_{Z/D})$, the total net charge of Y_Z-D1-His¹⁹⁰/Y_D-D2-His¹⁸⁹ was found to be +0.5/0.0. Thus, the radical pair Y[•]/Y⁻ is stabilized more for Y_Z than for Y_D. In the PSII crystal structure (1), both Y_Z and Y_D form H-bonds with N_ε of D1-His¹⁹⁰ and D2-His¹⁸⁹, respectively. N_δ of D1-His¹⁹⁰ is close to the side-chain oxygen of D1-Asn²⁹⁸ (Fig. 4). The N_δHis–O_{Asn} distance is 3.3:4.1 Å before/after constrained optimization of the atomic coordinates of the Y_Z-D1-His¹⁹⁰ pair in the reduced state. This contrasts with D2-His¹⁸⁹, whose N_δ forms a strong H-bond of salt-bridge character with the guanidinium nitrogens of the positively charged D2-Arg²⁹⁴ (N_δHis–N_εArg distance of 2.4 Å/3.2 Å and N_δHis–N_ηArg distance of 3.2 Å/ 3.5 Å before/after geometry optimization). The more distant N_η of this arginine is also involved in a strong salt-bridge with the acidic oxygen of CP47-Glu³⁶⁴ (N_ηArg–O_{Glu} distance of 2.9 Å) from the neighboring antenna complex CP47. Although the total net

charge of the salt-bridged pair, D2-Arg²⁹⁴ and CP47-Glu³⁶⁴ at Y_D vanishes, the two H-bonds from D2-Arg²⁹⁴ to N_δ at D2-His¹⁸⁹ do not allow this N_δ to be protonated.

Only for deprotonated D2-Arg²⁹⁴, N_δ of D2-His¹⁸⁹ could have a chance to protonate. But, due to the salt-bridge with CP47-Glu³⁶⁴, D2-Arg²⁹⁴ remains positively charged. Indeed, the calculated pK_a are ~15–17 for D2-Arg²⁹⁴ and ~0–2 for CP47-Glu³⁶⁴, independent of the Y_D redox state. Thus, protonation of D2-His¹⁸⁹ at N_δ is very unlikely. In fact, D2-Arg²⁹⁴ was fully protonated even when we removed the CP47 subunit. Contrary to D2-His¹⁸⁹, we observed N_δ of D1-His¹⁹⁰ to be permanently protonated, forming an H-bond with D1-Asn²⁹⁸. To estimate the influence of the positively charged D2-Arg²⁹⁴ on $E_m(Y_D)$, we also considered D2-Arg²⁹⁴ in its deprotonated neutral charged state and obtained $E_m(Y_D) = +823$ mV in the S2 state. The resulting upshift of 129 mV in $E_m(Y_D)$ demonstrates the significant role of the positively charged D2-Arg²⁹⁴ in lowering $E_m(Y_D)$, which may explain the remaining E_m difference of 100 mV between Y_Z and Y_D.

Although there was no report about an explicit role of D2-Arg²⁹⁴ in Y_D redox function, the importance of D2-Arg²⁹⁴ for stability and function of PSII was suggested from random mutagenesis studies of PSII from *Synechocystis* PCC 6803 (53). PSII mutated from D2-Arg²⁹⁴ to Trp was still capable of O₂ evolution but with a four-times-smaller initial rate, very sensitive to light, and rapid inhibition (53). An enhanced light-sensitivity, photoinhibition, and a limited ability to evolve O₂ were also observed in the CP47-Glu³⁶⁴ mutant for PsbV-depleted PSII, where D2-Arg²⁹⁴ is unable to form the salt-bridge with the residue Glu³⁶⁴ in CP47 (54). Among cyanobacteria and higher plants, the three residues D1-Asn²⁹⁸, D2-Arg²⁹⁴, and CP47-Glu³⁶⁴ are highly conserved. Thus, the asymmetry in protein sequence and structure of D1/D2 and CP43/CP47 proteins differentiates the function of Y_Z and Y_D by the H-bond and salt-bridge pattern.

Electrostatic interactions between Y_{Z/D} and P_{D1/D2}

So far all computations were performed for the neutral charged state of P_{D1/D2} i.e., P_{D1}⁰P_{D2}⁰. Here we report the influence of the other charge states at P_{D1/D2} on $E_m(Y_{Z/D})$. In general, an increase of the net charge in the proximity of a redox-active group upshifts its E_m . Thus, formation of P_{D1}⁺P_{D2}⁰ or P_{D1}⁰P_{D2}⁺ is expected to upshift $E_m(Y_{Z/D})$. Nevertheless, the calculated $E_m(Y_Z)$ remains almost unchanged among these P_{D1/D2} redox states, yielding values of +918 mV and +924 mV in the states P_{D1}⁺P_{D2}⁰ and P_{D1}⁰P_{D2}⁺, respectively (Table 3). In contrast, $E_m(Y_D)$ showed a remarkable upshift of 38 mV for P_{D1}⁺P_{D2}⁰ and 108 mV for P_{D1}⁰P_{D2}⁺. Thus, Y_D is much more sensitive to the redox state of P_{D1/D2} than Y_Z with a strong electrostatic link to P_{D2}.

The stronger interaction between Y_D and P_{D2} is likely due to the hydrophobic environment at Y_D as opposed to Y_Z, the latter having the polar Mn-cluster in its proximity (1). Furthermore, a cluster of titratable residues extends from

the Mn-cluster to the luminal surface (involving D1-Asp⁶¹, D1-Glu⁶⁵, D2-Lys³¹⁷, and D2-Glu³¹², and six residues of the PsbO protein, which are Asp^{O158}, Asp^{O222}, Asp^{O223}, Asp^{O224}, His^{O228}, and Glu^{O229}), forming a hydrophilic channel with D1-Asp⁶¹ at its mouth (5). On the other hand, the space near Y_D, which is equivalent to the position of the Mn-cluster at Y_Z, is filled with bulky hydrophobic residues (D2-Phe¹⁶⁸, D2-Phe¹⁸⁴, D2-Phe¹⁸⁵, D2-Phe¹⁸⁸, CP47-Phe³⁶², and CP47-Phe³⁶³) (5). These nontitratable residues cannot compensate for charges induced at Y_D or P_{D2}. Furthermore, the region between Y_D and P_{D2} seems to be relatively rigid. Thus, the low dielectric medium at Y_D/P_{D2} does not screen electrostatic interactions between Y_D and P_{D2}.

Faller et al. (7) measured the ET rate from Y_D to P680⁺ with a half-time of 180 ns (7). Their observed ET was much faster than that from earlier estimates (reviewed in (55)). To explain the kinetics of this ET process, they suggested that the cationic state of P680 should be localized on P_{D2} (7), where it can be pushed onto P_{D1} electrostatically if Y_D is in the oxidized state, thereby accelerating ET from Y_Z to P680⁺ (7,9). The specifically strong electrostatic interaction between Y_D and P_{D2}⁺ observed in our computations may corroborate these suggestions. Hence, presence of nontitratable residues in the neighborhood of Y_D/P_{D2} and their absence near to Y_Z/P_{D1} may be necessary to favor ET from Y_Z to P680⁺.

Influence of D2-Arg¹⁸⁰ on $E_m(Y_D)$

D2-Arg¹⁸⁰ is suggested to have an impact not only on P680 (12,56) but also on Y_D, because mutation of this residue led to a loss of EPR signal originated from the oxidized state of Y_D (57). To investigate the influence of this residue, we calculated $E_m(Y_{Z/D})$ in the S2 state in forcing D2-Arg¹⁸⁰ to be deprotonated. The resulting $E_m(Y_D)$ is +564 mV, significantly downshifted by 130 mV (Table 3). Surprisingly, $E_m(Y_Z)$ did not shift upon deprotonation of D2-Arg¹⁸⁰, confirming the EPR studies of D2-Arg¹⁸⁰ mutants (57) and thereby suggesting that this arginine has a predominant impact on Y_D but not Y_Z. To explain this large effect, it was previously proposed that D2-Arg¹⁸⁰ was capable of accepting a proton released from Y_D or stabilizing the proton on D2-His¹⁸⁹ (57). However, our computation yielded a pK_a of 11.3 for D2-Arg¹⁸⁰, which is standard for arginine. Hence, this arginine residue is generally protonated regardless of the redox states for P_{D1/D2} and Y_{Z/D}.

Indeed, the persistence of the D2-Arg¹⁸⁰ protonation is also one of the reasons that in our computation deprotonation/protonation by redox change at P_{D1/D2} and Y_D occurs predominantly at D2-His⁶¹. Interestingly, the symmetrical counterpart of D2-His⁶¹ is the acidic D1-Asp⁶¹, which is very close to the Mn-cluster, belonging to the hydrophilic channel leading to the luminal bulk surface (1,5,6). Both D1-Asp⁶¹ and D2-His⁶¹ are highly conserved among cyanobacteria and higher plants.

In the absence of light, the majority of PSII is adapted to the S1 state, not the lowest oxidized state S0 (58). This is probably due to the oxidative ability of Y_D (9,59). The corresponding $E_m(S1/S0)$ is estimated to be ~+700 mV (10,13). Since with deprotonated D2-Arg¹⁸⁰ the computed $E_m(Y_D)$ is only +564 mV, in a PSII mutant with depleted D2-Arg¹⁸⁰, Y_D might not be able to oxidize the S0 state to S1 efficiently. Hence, we suggest that the loss of EPR signal from Y_D in mutant PSII with depleted D1-Arg¹⁸⁰ can be associated with the inability of Y_D to oxidize the S0 to the S1 state. Therefore, Y_D in the wild-type PSII could play a redox-active role in photoassembly of the Mn-cluster as suggested in Rutherford et al. (9), and the ability to oxidize S0 to S1 by Y_D could depend on the value of $E_m(Y_D)$ with respect to $E_m(S1/S0)$.

CONCLUDING REMARKS

The calculated $E_m(Y/Y^-)$ were +926 mV/+694 mV for Y_Z/Y_D in S2 state of the Mn-cluster in agreement with former estimates (13,14). The differences in the distances of Y_Z and Y_D from the Mn-cluster as well as those in the H-bond network of Y_Z (Y_Z/D1-His¹⁹⁰/D1-Asn²⁹⁸) and Y_D (Y_D/D2-His¹⁸⁹/D2-Arg²⁹⁴/CP47-Glu³⁶⁴) are responsible for the differences in E_m . If D1-His¹⁹⁰ is protonated, $E_m(Y_Z/Y_Z^-) = +1216$ mV is nearly as high as $E_m(P680)$. $E_m(Y_ZH^+/Y_ZH)$ calculated in the Mn-depleted PSII model was +1264 mV, lower than that of +1576 mV calculated in intact PSII, implying that Y_ZH⁺/Y_ZH may serve as functional electron donor to P680⁺ in the Mn-depleted PSII as suggested by EPR spectroscopy on Mn-depleted PSII (50,51). CP43-Arg³⁵⁷ deprotonates as the S-state shifts from S0 to S2, suggesting its participation in water oxidation and proton translocation. A strong electrostatic link was found specifically between Y_D and P_{D2}. This is probably because of the presence of bulky hydrophobic residues (D2-Phe¹⁶⁸, D2-Phe¹⁸⁴, D2-Phe¹⁸⁵, D2-Phe¹⁸⁸, CP47-Phe³⁶², and CP47-Phe³⁶³) in the Y_D side. These residues cannot compensate for charges induced at Y_D or P_{D2}, in contrast to the hydrophilic residues likely serving as proton channel in the Y_Z side (D1-Asp⁶¹, D1-Glu⁶⁵, D2-Lys³¹⁷, D2-Glu³¹², and several residues of the PsbO protein). This difference in protein environment may explain the former suggestion that the cationic state of P680 should be localized on P_{D2} and can be pushed onto P_{D1} electrostatically, thereby accelerating ET from Y_Z to P680⁺ (7,9). The positively charged D2-Arg¹⁸⁰ upshifts $E_m(Y_D)$ significantly. Upshifting of $E_m(Y_D)$ by D2-Arg¹⁸⁰ might play a significant role in maintaining the redox ability of Y_D in intact PSII, as demonstrated by mutational studies (57).

SUPPLEMENTARY MATERIAL

An online supplement to this article can be found by visiting BJ Online at <http://www.biophysj.org>.

We thank Drs. Donald Bashford and Martin Karplus for providing the programs MEAD and CHARMM22, respectively. We thank Drs. Wolfram Saenger, Jacek Biesiadka, and Bernhard Loll for useful discussions.

This work was supported by the Deutsche Forschungsgemeinschaft grant No. SFB 498, Projects A5, Forschergruppe Project No. KN 329/5-1/5-2, grant No. GRK 80/2, grant No. GRK 268, and grant No. GRK 788/1. H.I. was supported by the Deutscher Akademischer Austauschdienst.

REFERENCES

1. Ferreira, K. N., T. M. Iverson, K. Maghlaoui, J. Barber, and S. Iwata. 2004. Architecture of the photosynthetic oxygen-evolving center. *Science*. 303:1831–1838.
2. Hoganson, C. W., and G. T. Babcock. 1997. A metalloradical mechanism for the generation of oxygen from water in photosynthesis. *Science*. 277:1953–1956.
3. Ahlbrink, R., M. Haumann, D. Cherepanov, O. Bogershausen, A. Mulikidjanian, and W. Junge. 1998. Function of tyrosine Z in water oxidation by photosystem II: electrostatic promoter instead of hydrogen abstractor. *Biochemistry*. 37:1131–1142.
4. Haumann, M., and W. Junge. 1999. Photosynthetic water oxidation: a simplex-scheme of its partial reactions. *Biochim. Biophys. Acta*. 1411: 86–91.
5. Barber, J., K. Ferreira, K. Maghlaoui, and S. Iwata. 2004. Structural model of the oxygen-evolving centre of photosystem II with mechanistic implications. *Phys. Chem. Chem. Phys.* 6:4737–4742.
6. Iwata, S., and J. Barber. 2004. Structure of photosystem II and molecular architecture of the oxygen-evolving centre. *Curr. Opin. Struct. Biol.* 14:447–453.
7. Faller, P., R. J. Debus, K. Brettel, M. Sugiura, A. W. Rutherford, and A. Boussac. 2001. Rapid formation of the stable tyrosyl radical in photosystem II. *Proc. Natl. Acad. Sci. USA*. 98:14368–14373.
8. Diner, B. A., and F. Rappaport. 2002. Structure dynamics, and energetics of the primary photochemistry of photosystem II of oxygenic photosynthesis. *Annu. Rev. Plant Biol.* 53:551–580.
9. Rutherford, A. W., A. Boussac, and P. Faller. 2004. The stable tyrosyl radical in photosystem II: why D? *Biochim. Biophys. Acta*. 1655: 222–230.
10. Tommos, C., and G. T. Babcock. 2000. Proton and hydrogen currents in photosynthetic water oxidation. *Biochim. Biophys. Acta*. 1458: 199–219.
11. Rappaport, F., M. Guergova-Kuras, P. J. Nixon, B. A. Diner, and J. Lavergne. 2002. Kinetics and pathways of charge recombination in photosystem II. *Biochemistry*. 41:8518–8527.
12. Ishikita, H., B. Loll, J. Biesiadka, W. Saenger, and E. W. Knapp. 2005. Redox potentials of chlorophylls in the photosystem II reaction center. *Biochemistry*. 44:4118–4124.
13. Vass, I., and S. Styring. 1991. pH-dependent charge equilibria between tyrosine-D and the S states in photosystem II. Estimation of relative midpoint redox potentials. *Biochemistry*. 30:830–839.
14. Boussac, A., and A. L. Etienne. 1982. Oxido-reduction kinetics of signal II slow in Tris-washed chloroplasts. *Biochem. Biophys. Res. Commun.* 109:1200–1205.
15. Brettel, K., E. Schlöder, and H. T. Witt. 1984. Nanosecond reduction kinetics of photooxidized chlorophyll-*a*_{II} (P-680) in single flashes as a probe for the electron pathway, H⁺-release and charge accumulation in the O₂-evolving complex. *Biochim. Biophys. Acta*. 766:403–415.
16. Tommos, C., X.-S. Tang, K. Warncke, C. W. Hoganson, S. Styring, J. McCracken, B. A. Diner, and G. T. Babcock. 1995. Spin-density distribution, conformation, and hydrogen bonding of the redox-active tyrosine Y_Z in photosystem II from multiple-electron magnetic-resonance spectroscopies: implications for photosynthetic oxygen evolution. *J. Am. Chem. Soc.* 117:10325–10335.
17. Haumann, M., A. Mulikidjanian, and W. Junge. 1999. Tyrosine-Z in oxygen-evolving photosystem II: a hydrogen-bonded tyrosinate. *Biochemistry*. 38:1258–1267.
18. Biesiadka, J., B. Loll, J. Kern, K.-D. Irrgang, and A. Zouni. 2004. Crystal structure of cyanobacterial photosystem II at 3.2 Å resolution: a closer look at the Mn-cluster. *Phys. Chem. Chem. Phys.* 6:4733–4736.
19. Ishikita, H., and E. W. Knapp. 2005. Control of quinone redox potentials in photosystem II: electron transfer and photoprotection. *J. Am. Chem. Soc.* 127:14714–14720.
20. Ishikita, H., and E. W. Knapp. 2005. Oxidation of the non-heme iron complex in photosystem II. *Biochemistry*. 44:14772–14783.
21. Brooks, B. R., R. E. Bruccoleri, B. D. Olafson, D. J. States, S. Swaminathan, and M. Karplus. 1983. CHARMM: a program for macromolecular energy minimization and dynamics calculations. *J. Comput. Chem.* 4:187–217.
22. MacKerell, A. D., Jr., D. Bashford, R. L. Bellott, R. L. Dunbrack, Jr., J. D. Evanseck, M. J. Field, S. Fischer, J. Gao, H. Guo, S. Ha, D. Joseph-McCarthy, L. Kuchnir, K. Kuczera, F. T. K. Lau, C. Mattos, S. Michnick, T. Ngo, D. T. Nguyen, B. Prodhom, W. E. Reiher III, B. Roux, M. Schlenkerich, J. C. Smith, R. Stote, J. Straub, M. Watanabe, J. Wierkiewicz-Kuczera, D. Yin, and M. Karplus. 1998. All-atom empirical potential for molecular modeling and dynamics studies of proteins. *J. Phys. Chem. B*. 102:3586–3616.
23. Popovic, D. M., A. Zmiric, S. D. Zaric, and E.-W. Knapp. 2002. Energetics of radical transfer in DNA photolyase. *J. Am. Chem. Soc.* 124:3775–3782.
24. Rabenstein, B., G. M. Ullmann, and E.-W. Knapp. 1998. Energetics of electron-transfer and protonation reactions of the quinones in the photosynthetic reaction center of *Rhodospseudomonas viridis*. *Biochemistry*. 37:2488–2495.
25. Popovic, D. M., S. D. Zaric, B. Rabenstein, and E.-W. Knapp. 2001. Artificial cytochrome *b*: computer modeling and evaluation of redox potentials. *J. Am. Chem. Soc.* 123:6040–6053.
26. Voigt, P., and E. W. Knapp. 2003. Tuning heme redox potentials in the cytochrome *c* subunit of photosynthetic reaction centers. *J. Biol. Chem.* 278:51993–52001.
27. Alexov, E. G., and M. R. Gunner. 1999. Calculated protein and proton motions coupled to electron transfer: electron transfer from Q_A⁻ to Q_B in bacterial photosynthetic reaction centers. *Biochemistry*. 38:8253–8270.
28. Zhu, Z., and M. R. Gunner. 2005. Energetics of quinone-dependent electron and proton transfers in *Rhodobacter sphaeroides* photosynthetic reaction centers. *Biochemistry*. 44:82–96.
29. Sugita, Y., N. Miyashita, M. Ikeguchi, A. Kidera, and C. Toyoshima. 2005. Protonation of the acidic residues in the transmembrane cation-binding sites of the Ca²⁺ pump. *J. Am. Chem. Soc.* 127:6150–6151.
30. Rabenstein, B., G. M. Ullmann, and E.-W. Knapp. 1998. Calculation of protonation patterns in proteins with structural relaxation and molecular ensembles—application to the photosynthetic reaction center. *Eur. Biophys. J.* 27:626–637.
31. Steffen, M. A., K. Lao, and S. G. Boxer. 1994. Dielectric asymmetry in the photosynthetic reaction center. *Science*. 264:810–816.
32. Bashford, D., and M. Karplus. 1990. pK_a's of ionizable groups in proteins: atomic detail from a continuum electrostatic model. *Biochemistry*. 29:10219–10225.
33. Ishikita, H., B. Loll, J. Biesiadka, A. Galstyan, W. Saenger, and E.-W. Knapp. 2005. Tuning electron transfer by ester-group of chlorophylls in bacterial photosynthetic reaction center. *FEBS Lett.* 579:712–716.
34. Ishikita, H., and E. W. Knapp. 2005. Induced conformational change upon Cd²⁺ binding at photosynthetic reaction centers. *Proc. Natl. Acad. Sci. USA*. 102:16215–16220.
35. Ishikita, H., D. Stehlik, J. H. Golbeck, and E.-W. Knapp. 2006. Electrostatic influence of PsaC protein binding to the PsaA/PsaB heterodimer in photosystem I. *Biophys. J.* 90:1081–1089.
36. Hendry, G., and T. Wydrzynski. 2003. ¹⁸O isotope exchange measurements reveal that calcium is involved in the binding of one

- substrate-water molecule to the oxygen-evolving complex in photosystem II. *Biochemistry*. 42:6209–6217.
37. McEvoy, J. P., and G. W. Brudvig. 2004. Structure-based mechanism of photosynthetic water oxidation. *Phys. Chem. Chem. Phys.* 6:4754–4763.
 38. Rutherford, A. W., and A. Boussac. 2004. Water photolysis in biology. *Science*. 303:1782–1784.
 39. Candeias, L. P., S. Turconi, and J. H. A. Nugent. 1998. Tyrosine Y_Z and Y_D of photosystem II: comparison of optical spectra to those of tyrosine oxidised by pulsed radiolysis. *Biochim. Biophys. Acta*. 1363:1–5.
 40. Diner, B. A., D. A. Force, D. W. Randall, and R. D. Britt. 1998. Hydrogen bonding, solvent exchange, and coupled proton and electron transfer in the oxidation and reduction of redox-active tyrosine Y_Z in Mn-depleted core complexes of photosystem II. *Biochemistry*. 37:17931–17943.
 41. Noguchi, T., Y. Inoue, and X.-S. Tang. 1997. Structural coupling between the oxygen-evolving Mn cluster and a tyrosine residue in photosystem II as revealed by Fourier transform infrared spectroscopy. *Biochemistry*. 36:14705–14711.
 42. Berthomieu, C., R. Hienerwadel, A. Boussac, J. Breton, and B. A. Diner. 1998. Hydrogen bonding of redox-active tyrosine Z of photosystem II probed by FTIR difference spectroscopy. *Biochemistry*. 37:10547–10554.
 43. Högbom, M., M. Galander, M. Andersson, M. Kolberg, W. Hofbauer, G. Lassmann, P. Nordlund, and F. Lendzian. 2003. Displacement of the tyrosyl radical cofactor in ribonucleotide reductase obtained by single-crystal high-field EPR and 1.4-Å x-ray data. *Proc. Natl. Acad. Sci. USA*. 100:3209–3214.
 44. Faller, P., C. Goussias, A. W. Rutherford, and S. Un. 2003. Resolving intermediates in biological proton-coupled electron transfer: a tyrosyl radical pair to proton movement. *Proc. Natl. Acad. Sci. USA*. 100:8732–8735.
 45. Tommos, C., J. J. Skalicky, D. L. Pilloud, A. J. Wand, and P. L. Dutton. 1999. De novo proteins as models of radical enzymes. *Biochemistry*. 38:9495–9507.
 46. Geijer, P., F. Morvaridi, and S. Styring. 2001. The S₃ state of the oxygen-evolving complex in photosystem II is converted to the S₂Y_Z state at alkaline pH. *Biochemistry*. 40:10881–10891.
 47. Petrouleas, V., D. Koulougliotis, and N. Ioannidis. 2005. Trapping of metalloradical intermediates of the S-states at liquid helium temperatures. Overview of the phenomenology and mechanistic implications. *Biochemistry*. 44:6723–6728.
 48. Hays, A.-M. A., I. R. Vassiliev, J. H. Golbeck, and R. J. Debus. 1998. Role of D1-His¹⁹⁰ in proton-coupled electron transfer reactions in photosystem II: a chemical complementation study. *Biochemistry*. 37:11352–11365.
 49. Diner, B. A. 2001. Amino acid residues involved in the coordination and assembly of the manganese cluster of photosystem II. Proton-coupled electron transport of the redox-active tyrosines and its relationship to water oxidation. *Biochim. Biophys. Acta*. 1503:147–163.
 50. Astashkin, A. V., H. Mino, A. Kawamori, and T.-A. Ono. 1997. Pulsed EPR study of the S₃ signal in the Ca²⁺-depleted photosystem II. *Chem. Phys. Lett.* 272:506–516.
 51. Mino, H., and A. Kawamori. 2001. EPR studies of the water oxidizing complex in the S₁ and the higher S states: the manganese cluster and Y_Z radical. *Biochim. Biophys. Acta*. 1503:112–122.
 52. Knoepfle, N., T. M. Bricker, and C. Putnam-Evans. 1999. Site-directed mutagenesis of basic arginine residues 305 and 342 in the CP43 protein of photosystem II affects oxygen-evolving activity in *Synechocystis* 6803. *Biochemistry*. 38:1582–1588.
 53. Ermakova-Gerdes, S., Z. Yu, and W. Vermaas. 2001. Targeted random mutagenesis to identify functionally important residues in the D2 protein of photosystem II in *Synechocystis* sp. strain PCC 6803. *J. Bacteriol.* 183:145–154.
 54. Morgan, T. R., J. A. Shand, S. M. Clarke, and J. J. Eaton-Rye. 1998. Specific requirements for cytochrome c-550 and the manganese-stabilizing protein in photoautotrophic strains of *Synechocystis* sp. PCC 6803 with mutations in the domain Gly-351 to Thr-436 of the chlorophyll-binding protein CP47. *Biochemistry*. 37:14437–14449.
 55. Diner, B. A., and G. T. Babcock. 1996. Oxygenic Photosynthesis: The Light Reactions. D.R. Ort and C.F. Yocum, editors. Kluwer Academic Publishers, Dordrecht, Netherlands. 213–247.
 56. Mulikjanian, A. Y. 1999. Photosystem II of green plants: on the possible role of retarded protonic relaxation in water oxidation. *Biochim. Biophys. Acta*. 1410:1–6.
 57. Manna, P., R. LoBrutto, C. Eijkelhoff, J. P. Dekker, and W. Vermaas. 1998. Role of Arg¹⁸⁰ of the D2 protein in photosystem II structure and function. *Eur. J. Biochem.* 251:142–154.
 58. Joliot, P., A. Joliot, and B. Kok. 1968. Analysis of the interactions between the two photosystems in isolated chloroplasts. *Biochim. Biophys. Acta*. 153:635–652.
 59. Styring, S., and A. W. Rutherford. 1987. In the oxygen-evolving complex of photosystem II the S₀ state is oxidized to the S₁ state by D⁺ (signal I_{slow}). *Biochemistry*. 26:2401–2405.